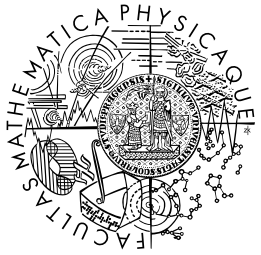

FACULTY
OF MATHEMATICS
AND PHYSICS
Charles University

BACHELOR THESIS

Jan Jerhot

Study of rare decays at NA62 experiment in CERN

Institute of Particle and Nuclear Physics

Supervisor of the bachelor thesis:	Mgr. Michal Zamkovský
Co-supervisor:	doc. RNDr. Karol Kampf, PhD.
Study programme:	Physics
Study branch:	General physics

Prague 2017

I declare that I carried out this bachelor thesis independently, and only with the cited sources, literature and other professional sources.

I understand that my work relates to the rights and obligations under the Act No. 121/2000 Sb., the Copyright Act, as amended, in particular the fact that the Charles University has the right to conclude a license agreement on the use of this work as a school work pursuant to Section 60 subsection 1 of the Copyright Act.

In ..... date ..... signature of the author

Title: Study of rare decays at NA62 experiment in CERN

Author: Jan Jerhot

Institute: Institute of Particle and Nuclear Physics

Supervisor: Mgr. Michal Zamkovský, Institute of Particle and Nuclear Physics

Co-supervisor: doc. RNDr. Karol Kampf, PhD., Institute of Particle and Nuclear Physics

Abstract: The subject of this thesis is the study of a rare $\pi^0 \to \nu\bar{\nu}$ decay. The first part of this thesis contains the evaluation of the branching ratio of this decay using the precisely measured dominant $\pi^0 \to \gamma\gamma$ decay and a discussion of the theoretical background. Then in the second part is a preparation for the experimental measurement of this decay which is divided to a description of an experiment and used apparatus and the data analysis from the $K^+ \to \pi^+\pi^0$ decay on data from the 2016 run. Specifically the efficiency of the calorimeter for the dominant $\pi^0 \to \gamma\gamma$ decay is analysed.

Keywords: standard model, rare decays, branching ratio, NA62 experiment, efficiency

I would like to express my sincere gratitude to my supervisor, Michal Zamkovsky, for an opportunity to work on an international experiment, for his guidance during the data analysis and immense patience. I would also like to thank Karol Kampf for discussions about theoretical issues of this thesis and members of the NA62 collaboration for helping me with the practical part of the thesis.

Especially I want to thank my family and friends for their love and huge support during my whole bachelor's studies.

Contents

Introduction **3**

1 Theory **5**
1.1 Standard Model . . . 5
1.1.1 Particle families . . . 5
1.1.2 Particle interactions . . . 6
1.2 Mesons and π^0 . . . 8
1.3 Kinematics . . . 9
1.4 Studied decay . . . 10
1.4.1 $\pi^0 \to \gamma\gamma$ decay width . . . 11
1.4.2 $\pi^0 \to \nu\bar{\nu}$ decay width . . . 11
1.4.3 Branching ratio evaluation . . . 13

2 Layout of NA62 experiment **15**
2.1 The aim of NA62 . . . 17
2.2 Beam line . . . 17
2.3 KTAG/CEDAR . . . 17
2.4 GTK . . . 18
2.5 CHANTI . . . 19
2.6 Decay region and LAVs . . . 20
2.7 Straw Spectrometer . . . 21
2.8 RICH . . . 22
2.9 CHOD/NewCHOD . . . 24
2.10 LKr . . . 25
2.11 MUV . . . 25
2.12 Additional Veto Detectors . . . 26

3 Trigger system **27**
3.1 L0 trigger . . . 27
3.2 High level triggers . . . 28
3.2.1 L1 trigger . . . 28
3.2.2 L2 trigger . . . 28

4 Data analysis **29**
4.1 Reconstruction strategy . . . 29
4.1.1 Tracks reconstruction . . . 29
4.1.2 Event reconstruction . . . 31
4.2 $\pi^0 \to \gamma\gamma$ decay reconstruction . . . 31

Conclusion **37**

Bibliography **39**

List of Abbreviations **41**

Introduction

While we are limited by reachable energy in terms of collisions, no such limitation holds for rare decays. Therefore the study of rare kaon and pion decays is a good opportunity to search for a new physics beyond the standard model. Especially low energy events (like pion decays) are very precisely described by the chiral perturbation theory (χPT) corrections for the standard model. Experimentally measured deviations from the model gives plenty of space for a new physics due to this remarkable theoretical precision.

The main goal of NA62 experiment in CERN is to measure the rare $K^+ \to \pi^+\nu\bar{\nu}$ decay which theoretical branching ratio is [1]

$$BR(K^+ \to \pi^+\nu\bar{\nu}) = (8.4 \pm 1.0) \cdot 10^{-11}, \tag{1}$$

however the experimental value from the E949 collaboration in the Brookhaven National Laboratory (BNL) is [2]

$$BR(K^+ \to \pi^+\nu\bar{\nu}) = (1.75\ ^{+\ 1.15}_{-\ 1.05}) \cdot 10^{-10}. \tag{2}$$

The theoretical result lies on the border of experimental error, if there will be a gap between theory and experiment after more precise measurements, it is a clear sign of physics beyond standard model. The main goal of NA62 is to contribute to investigation of CP-violation and the strength of flavor-changing weak decays described by Cabibbo–Kobayashi–Maskawa (CKM) mixing matrix by measuring the $|V_{td}|$ element of the CKM matrix with 10% error or lower [3].

Since the decay $K^+ \to \pi^+\pi^0$ is represented with significant branching ratio, the experiment also provides opportunity to measure rare pion decays, like $\pi^0 \to \nu\bar{\nu}$, which is the subject of this thesis.

The first reason to study this decay is the spatial indistinguishability of the $K^+ \to \pi^+\nu\bar{\nu}$ decay from the $K^+ \to \pi^+\pi^0$ and $\pi^0 \to \nu\bar{\nu}$ decay, which then constitutes background. The second reason is the sensitivity of the measurement to any $\pi^0 \to$ "nothing" decays arising from processes beyond standard model, like decay to neutrinos of different flavor, right-handed neutrinos or any other weakly interacting neutral states which can be for example hypothetical dark matter candidates.

While the theoretical upper limit on the branching ratio of this decay (evaluated in 1.4.3) is

$$BR(\pi^0 \to \nu\bar{\nu}) < 5 \cdot 10^{-10} \tag{3}$$

the experimental upper limit from BNL - E949 collaboration [4] is

$$BR(\pi^0 \to \nu\bar{\nu}) < 2.7 \cdot 10^{-7}. \tag{4}$$

The subject of this thesis is in the first part to demonstrate the evaluation of the theoretical branching ratio upper limit using χPT results and to discuss

limits of its validity.

The setup of the NA62 experiment and a basic preparation of the fundamental data analysis for possible future branching ratio evaluation from NA62 data is shown in the second part of the thesis.

1. Theory

1.1 Standard Model

The Standard Model of particle physics (SM) is a theory of elementary particles and interactions among them, except of gravity. The organization of SM can be seen in the figure 1.1

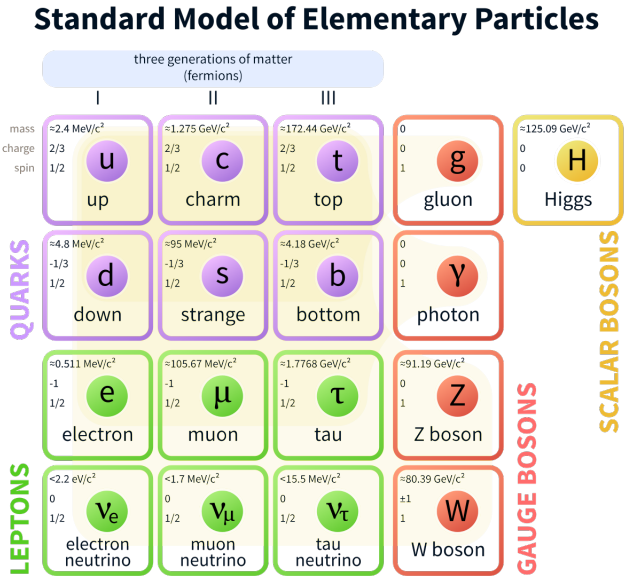

Figure 1.1: Standard Model of particle physics [22].

1.1.1 Particle families

All elementary particles have an intrinsic angular momentum called quantum spin number S or just spin. As it is quantizatied and elementary particles are thought as single points, it has no direct analogy in classical physics. S is any whole number multiple of a half. Most generally are particles divided on fermions and bosons where fermions have a half integral spin and bosons have an integral spin number. No spin numbers are possible between these. Fermions are described by Fermi-Dirac statistics and obey Pauli exclusion principle. On the other hand bosons are described by Bose-Einstein statistics.

The elementary bosons mediate interactions. Gluons, photons, and the W and Z bosons are forces carrying bosons of the standard model (see gauge bosons in the figure 1.1) and have a spin 1 because they correspond to vector fields. The Higgs boson goes with a scalar field so it has a zero spin. If the graviton as a mediator of the gravitational field is ever discovered, it is expected to have a spin 2 since it corresponds to a tensor field.

The elementary fermions are fundamental structures of matter and have a spin ½. Particles made from combinations of fermions will have an overall spin given as a sum of individual spins. The elementary fermions are divided into two groups (quarks and leptons) in three known generations: from ordinary (I), to exotic (II), to very exotic (III) - see figure 1.1.

Quarks are fermions which must bind together, they are known to bind into colorless triplets and pairs. The triplets are called baryons and are composed of three quarks, which give an overall spin of ½ or ³⁄₂, since those are the only possible, non-negative combinations of ½. Therefore all baryons (like protons and neutrons, for example) are also fermions. The pairs are called mesons and are composed of a quark and an antiquark, which will combine to an overall spin of 0 or 1 since those are the only possible, non-negative combinations of ½ ± ½. This shows that mesons (like a pion) are also bosons. In three known generations there are six flavors (types) of quarks known: up u, down d, strange s, charm c, top t, and bottom b.

Compositions of quarks are collectively called hadrons. Therefore baryons (the heavy triplets) and mesons (the middleweight doublets) are hadrons. There are also exotic hadrons like tetraquarks and pentaquarks. Especially baryons found in the nucleus (the proton and neutron) are called nucleons. Baryons that contain at least one strange quark but no charm, bottom, or top quarks are called hyperons.

The other six fermions which can exist independently are called leptons. Originally leptons were considered the "light" particles and hadrons the "heavy" particles, but the discovery of the tau lepton broke that rule (tau is almost twice as massive as a proton). The neutrinos are an important subgroup within the leptons. They come in three flavors named by their partner leptons - the electron, muon, and tau are matched with the electron neutrino, muon neutrino, and tau neutrino. Neutrinos have very little mass (even for leptons) and interact so weakly with the rest of the particles that they are exceptionally difficult to detect.

1.1.2 Particle interactions

Three from four fundamental forces are described by SM - electromagnetism, the strong force, and the weak force. Each of these forces acts between particles with some special attribute and as was mentioned these forces are mediated by gauge bosons. For electromagnetism the charge is this attribute and is mediated by photons (γ), color charge for the strong force mediated by gluons (g) and flavor for the weak force mediated by $W^{\pm}$ and Z^0 bosons.

Charge is an attribute of matter which stands behind electric and magnetic phenomena, known collectively as electromagnetism. Charge can exist only in integral multiples of elementary charge. The only exception are quarks which carry fractions of the elementary charge but are always bind into composite particles of integral multiple of the elementary charge, so fractional charge has never

been directly measured. Charged particles interact through exchange of photons which are massless, uncharged, and have an unlimited range. The mathematical model used to describe the interaction of charged particles through the exchange of photons is known as quantum electrodynamics (QED).

The strong interaction binds quarks together into hadrons as they have a characteristic known as color (or color charge) and also the residual strong force binds nucleons together through exchange of virtual mesons. Quarks come in one of three colors and anticolors: $\pm$ red (r), $\pm$ green (g), and $\pm$ blue (b) and forms 'color neutral' matter in terms of rule: $g + \bar{g} = r + \bar{r} = b + \bar{b} = 0$, $g + r + b = 0$, $\bar{g} + \bar{r} + \bar{b} = 0$. Colored particles are bound together by gluons which are also colored, but in a different way than the quarks are. Six of the eight gluons have two colors, one has four, and another has six, therefore they also stick to themselves, which consequence is that they are short distant, see figure 1.2. The mathematical model used to describe the interaction of colored particles through the exchange of gluons is known as quantum chromodynamics (QCD).

As we can see in the figure 1.1, fermions comes in twelve different flavors. Flavored particles interact weakly through the exchange of $W^{\pm}$ or Z^0 bosons, so if a flavor of an elementary fermion changes, the weak force is responsible. The mathematical model used to describe the interaction of flavored particles through the exchange of $W^{\pm}$ and Z^0 bosons is sometimes known as quantum flavordynamics, but this term is not much used. At higher energies, the weak and electromagnetic forces begin to look more alike, so the conventional name for the theory of the weak force is electroweak theory (EWT).

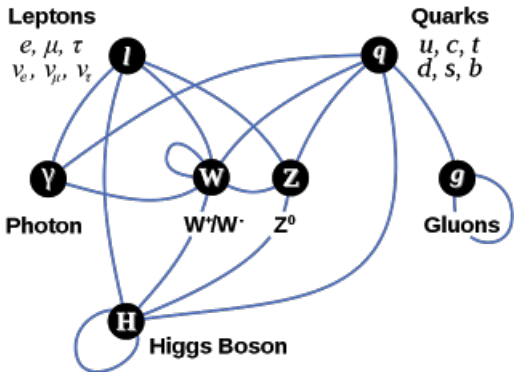

Figure 1.2: Map of interactions [23].

Because some particles are massless (like photons and gluons) and some not, it was believed that there is another interaction that some particles feel and others do not. Nowadays the interaction that gives mass to elementary particles is called the Higgs mechanism and the particle that mediates the interaction is called the Higgs boson H. The quarks, leptons, and $W^{\pm}$ and Z^0 bosons moving through the space interact with the scalar Higgs field, which is why these particles have a mass. On the other hand photons and gluons do not interact with the Higgs field, thus they are massless. Even the Higgs boson itself interacts with the Higgs field as it has mass, see figure 1.2. The Higgs boson is different from the other

bosons (gluons, photons, $W^{\pm}$ and Z^0 bosons) because the Higgs mechanism does not result in anything resembling a force (like the strong, electromagnetic, and weak forces), the Higgs field is a scalar field and the Higgs boson is a particle with zero spin [5].

1.2 Mesons and π^0

As was mentioned in the introduction, the main goal of NA62 experiment is to measure rare decays of kaon, especially the $K^+ \to \pi^+\nu\bar{\nu}$ decay. Kaons K are mesons, more precisely mesons with strange quark. There are four types of kaon depending on configuration of quarks [6]:

Symbol	Quark content	Mass (MeV/c)	Mean lifetime (s)
K^+	$u\bar{s}$	493.677 ± 0.016	$(1.2380 \pm 0.0020) \cdot 10^{-8}$
K^-	$\bar{u}s$	493.677 ± 0.016	$(1.2380 \pm 0.0020) \cdot 10^{-8}$
K^0_S	$\frac{d\bar{s} + \bar{d}s}{\sqrt{2}}$	497.611 ± 0.013	$(0.8954 \pm 0.0004) \cdot 10^{-10}$
K^0_L	$\frac{d\bar{s} - \bar{d}s}{\sqrt{2}}$	497.611 ± 0.013	$(5.116 \pm 0.021) \cdot 10^{-8}$

Table 1.1: Properties of kaons

Because the branching ratio of $K^+ \to \pi^+\pi^0$ decay is $BR(K^+ \to \pi^+\pi^0) = (20.67 \pm 0.08)\%$, the experiment is also a good opportunity to measure rare $\pi^0 \to \nu\bar{\nu}$ decay which also creates background for measuring $K^+ \to \pi^+\nu\bar{\nu}$. The $\pi^0 \to \nu\bar{\nu}$ is the object of our study. π^0 is a π meson or pion, where pions are the lightest mesons and are composed of u and d quarks [6]:

Symbol	Quark content	Mass (MeV/c)	Mean lifetime (s)
π^+	$u\bar{d}$	139.57018 ± 0.00035	$(2.6033 \pm 0.0005) \cdot 10^{-8}$
π^-	$\bar{u}d$	139.57018 ± 0.00035	$(2.6033 \pm 0.0005) \cdot 10^{-8}$
π^0	$\frac{u\bar{u} - \bar{d}d}{\sqrt{2}}$	134.9766 ± 0.0006	$(8.52 \pm 0.18) \cdot 10^{-17}$

Table 1.2: Properties of pions

Pions, kaons and η mesons are *pseudoscalar mesons*, which means that they have zero total spin and odd parity. η and η' mesons are composed of up, down and strange quarks.

Symbol	Quark content	Mass (MeV/c)	Mean lifetime (s)
η	$\frac{u\bar{u}+d\bar{d}-2s\bar{s}}{\sqrt{6}}$	547.862 ± 0.018	$(5.0 \pm 0.3) \cdot 10^{-19}$
η'	$\frac{u\bar{u}+d\bar{d}+s\bar{s}}{\sqrt{3}}$	957.78 ± 0.06	$(3.2 \pm 0.2) \cdot 10^{-21}$

Table 1.3: Properties of η mesons

Pions, kaons and η mesons together forms *pseudoscalar nonet* or *pseudoscalar octet* without the η' state.

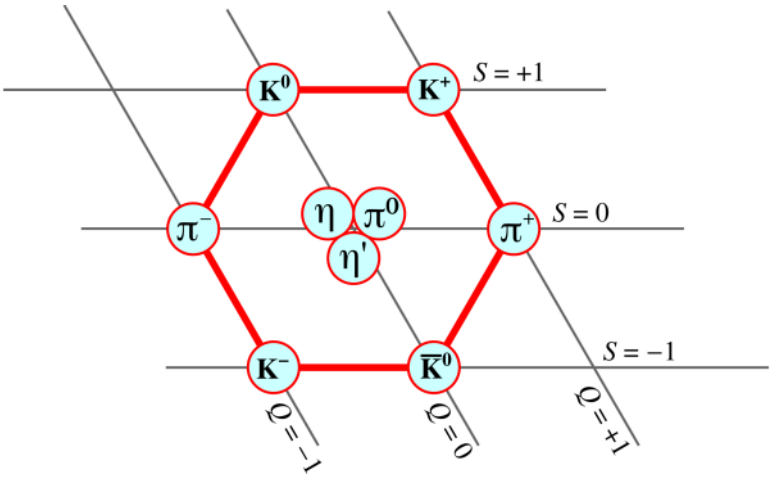

Figure 1.3: Nonet of pseudoscalar mesons [24].

1.3 Kinematics

To evaluate the branching ratio of the $\pi^0 \to \nu\bar{\nu}$ decay from kinematics, several concepts has to be defined.

We have the $E^2 = \boldsymbol{p}^2 + m^2$ relation from the definition of relativistic energy, which can be in differential form written as

$$(\Box + m^2)\psi(x) = 0, \ \boldsymbol{p} \to -i\nabla, \ E \to i\frac{\partial}{\partial t}, \tag{1.1}$$

which is called *Klein-Gordon equation* and can be interpreted as single-particle wave equation. In relativistic mechanics the negative energy solutions could be ignored, nevertheless in quantum mechanics we have to keep the complete set of solutions. Thus Dirac has rewritten the equation using the *gamma matrices* which are in the Dirac representation:

$$\gamma^0 = \begin{pmatrix} \mathbb{1}_2 & 0 \\ 0 & -\mathbb{1}_2 \end{pmatrix}, \ \gamma^i = \begin{pmatrix} 0 & \sigma^i \\ -\sigma^i & 0 \end{pmatrix} \tag{1.2}$$

where σ^i are *Pauli matrices*:

$$\sigma^x = \begin{pmatrix} 0 & 1 \\ 1 & 0 \end{pmatrix}, \ \sigma^y = \begin{pmatrix} 0 & -i \\ i & 0 \end{pmatrix}, \ \sigma^z = \begin{pmatrix} 1 & 0 \\ 0 & -1 \end{pmatrix} \tag{1.3}$$

Anticommutator relations for gamma matrices are

$$\{\gamma^\mu, \gamma^\nu\} = 2g^{\mu\nu},\ g^{\mu\nu} = \begin{pmatrix} 1 & 0 & 0 & 0 \\ 0 & -1 & 0 & 0 \\ 0 & 0 & -1 & 0 \\ 0 & 0 & 0 & -1 \end{pmatrix} \tag{1.4}$$

and we will also define fifth gamma matrix γ^5 as

$$\gamma^5 := i\gamma^0\gamma^1\gamma^2\gamma^3 \overset{\text{Dirac rep.}}{=} \begin{pmatrix} 0 & \mathbb{1}_2 \\ \mathbb{1}_2 & 0 \end{pmatrix}. \tag{1.5}$$

The equation (1.1) can be then rewritten as *Dirac equation*

$$(i\gamma^\mu\partial_\mu - m)\psi(x) = 0, \tag{1.6}$$

where $\psi(x)$ has now four components and is called the *Dirac spinor*. Other often used representations are the *Weyl (or chiral) representation* used for ultra-relativistic cases and the *Majorana representation* which makes the Dirac equation (1.6) real and is helpful for *Majorana fermions* where particles are equal to antiparticles.

Because Dirac spinors satisfy the Klein-Gordon equation (1.1), we can define

$$\psi(x) = u(\boldsymbol{p})e^{-ipx}, \tag{1.7}$$

which after inclusion into the Dirac equation (1.6) gives the *momentum space Dirac equation*

$$(\not{p} - m)u(\boldsymbol{p}, \sigma) = 0, \tag{1.8}$$

which has two positive energy solutions (for two polarizations σ) for spinor $u(\boldsymbol{p}, \sigma)$ and two negative energy solutions. Negative-energy solutions are interpreted as positive-energy antiparticle solutions for momentum space Dirac equation

$$(\not{p} + m)v(\boldsymbol{p}, \sigma) = 0 \tag{1.9}$$

for spinor $v(\boldsymbol{p}, \sigma)$ [7]. Where *Feynman slash notation* was used:

$$\not{A} := \gamma^\mu A_\mu \tag{1.10}$$

1.4 Studied decay

The partial decay width of particle with mass M into n bodies is given by [6]

$$d\Gamma = \frac{(2\pi)^4}{2M} \left|\mathscr{M}\right|^2 d\Phi_n(\boldsymbol{P}; \boldsymbol{p}_1, ..., \boldsymbol{p}_n) \tag{1.11}$$

where $|\mathscr{M}|$ is an amplitude and $d\Phi_n$ is an element of n-body phase space. Especially for two-body decays the phase space is very simple.

1.4.1 $\pi^0 \to \gamma\gamma$ decay width

As the branching ratio for $\pi^0 \to \gamma\gamma$ is well measured - $BR(\pi^0 \to \gamma\gamma) = (98.823 \pm 0.034)\%$ [6], we can use the decay width of this decay for calculating the branching ratio of our decay $\pi^0 \to \nu\bar{\nu}$. The low-energy interactions of the pseudoscalar octet (see figure 1.3) are well described by the *Chiral perturbation theory* (χPT) [8]. For the $\pi^0 \to \gamma\gamma$ decay we have the partial decay width

$$\Gamma_{\gamma\gamma} = \frac{\pi}{4}\alpha^2 M_{\pi^0}^3 \left|T\right|^2, \tag{1.12}$$

where T is reduced amplitude and α is the fine-structure constant. With χPT the amplitude can be evaluated - for for us sufficient precision we will use the leading order (LO) corrections for chiral anomaly:

$$F_\pi T_{LO} = \frac{1}{4\pi^2}, \tag{1.13}$$

where F_π is the pion decay constant $\sqrt{2}F_\pi = 130.2(1.7)$ MeV [10] ($\sqrt{2}$ due to the convention). For more precise result, which includes one and two loops solutions, next-to-leading order (NLO) and next-to-next-to-leading order (NNLO) corrections are evaluated in [11]. The $\Gamma_{\gamma\gamma}$ can be now evaluated from (1.12) as

$$\Gamma_{\gamma\gamma} = \frac{\pi}{4}\alpha^2 M_{\pi^0}^3 \left|T\right|^2 \approx \frac{\pi}{4}\alpha^2 M_{\pi^0}^3 \frac{1}{F_\pi^2}\frac{1}{(4\pi)^2} = \frac{1}{(4\pi)^3}\alpha^2 M_{\pi^0}^3 \frac{1}{F_\pi^2} \tag{1.14}$$

1.4.2 $\pi^0 \to \nu\bar{\nu}$ decay width

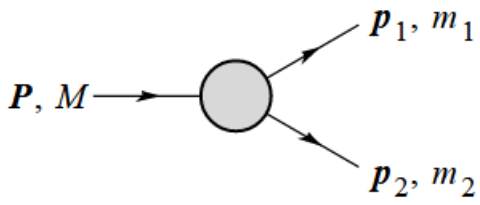

Figure 1.4: Definitions of variables for two-body decay [6].

The $\pi^0 \to \nu\bar{\nu}$ is also a two-body decay, so from kinematics [6] we have

$$E_1 = \frac{M^2 - m_2^2 + m_1^2}{2M} \tag{1.15}$$

$$|\boldsymbol{p}_1| = |\boldsymbol{p}_2| = \frac{\sqrt{(M^2 - (m_1 + m_2)^2)(M^2 - (m_1 - m_2)^2)}}{2M} \tag{1.16}$$

and from general relation (1.11):

$$d\Gamma = \frac{1}{32\pi^2}\left|\mathscr{M}\right|^2 \frac{|\boldsymbol{p}_1|}{M^2} d\Omega. \tag{1.17}$$

Thus for angle-independent momentum, we can integrate (1.17) and get

$$\Gamma = \frac{1}{32\pi^2}\left|\mathscr{M}\right|^2 \frac{|\boldsymbol{p}_1|}{M^2} 4\pi = \frac{1}{8\pi}\left|\mathscr{M}\right|^2 \frac{|\boldsymbol{p}_1|}{M^2}. \tag{1.18}$$

As pion is the decayed particle, we get $M = M_{\pi^0}$ and both neutrinos masses are the same $m_{1,2} = m_\nu$. The relation (1.16) is then

$$|\boldsymbol{p}| = \frac{\sqrt{(M_{\pi^0}^2 - 4m_\nu)M_{\pi^0}^2}}{2M_{\pi^0}} = \frac{M_{\pi^0}}{2}\sqrt{1 - \frac{4m_\nu^2}{M_{\pi^0}^2}}. \tag{1.19}$$

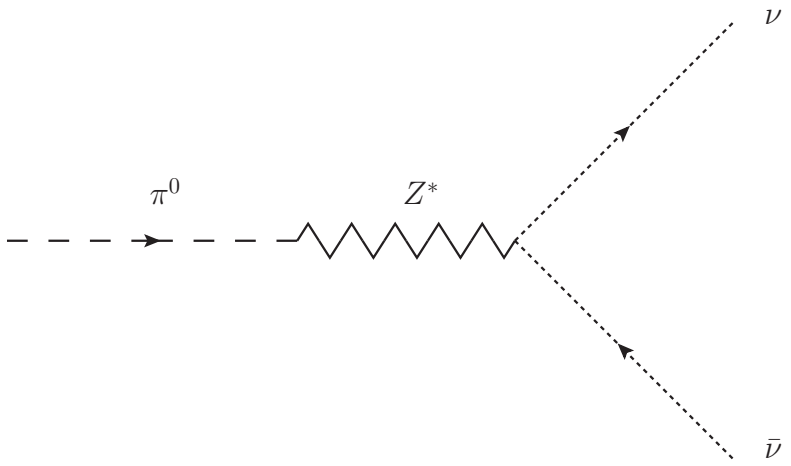

Figure 1.5: Feynman diagram of the decay

The amplitude $|\mathscr{M}|$ can be derived from the Feynman diagram 1.5 using Feynman rules

$$\mathscr{M}^{\text{weak}}_{\pi^0 \to \nu\bar{\nu}} = \sqrt{2} G_F F_\pi m_\nu \bar{u}\gamma^5 v, \tag{1.20}$$

where $u(\boldsymbol{p})$ is a spinor of ν with momentum $\boldsymbol{p}$ and $v(\boldsymbol{q})$ is a spinor of $\bar{\nu}$ with momentum $\boldsymbol{q}$. $\sqrt{2}F_\pi$ is the pion decay constant [10] and G_F is the Fermi coupling constant $G_F = 1.166\ 387\ 7(6) \cdot 10^{-5}\ \text{GeV}^{-2}$ [6]. For squared then

$$\begin{aligned} |\mathscr{M}|^2 &= \mathscr{M}\mathscr{M}^* = 2G_F^2 F_\pi^2 m_\nu^2 \bar{u}\gamma^5 v \bar{v}\gamma^5 u = \\ &= 2G_F^2 F_\pi^2 m_\nu^2\ \text{Tr}(\bar{u}\gamma^5 v \bar{v}\gamma^5 u) = 2G_F^2 F_\pi^2 m_\nu^2\ \text{Tr}(u\bar{u}\gamma^5 v \bar{v}\gamma^5). \end{aligned} \tag{1.21}$$

For $u\bar{u}$ holds for both polarizations:

$$\sum_{\sigma=1,2} u(\boldsymbol{p},\sigma)\bar{u}(\boldsymbol{p},\sigma) = \not{p} + m$$
$$\sum_{\sigma=1,2} v(\boldsymbol{q},\sigma)\bar{v}(\boldsymbol{q},\sigma) = \not{q} - m$$

as we consider just one helicity for neutrinos and $M_{\pi^0}^2$ is two degrees larger than m_ν^2 (for ν_τ, for other flavours even more), we can substitute:

$$|\mathscr{M}|^2 = 2G_F^2 F_\pi^2 m_\nu^2\ \text{Tr}(\not{p}\not{q}\gamma^5\gamma^5). \tag{1.22}$$

Because of $\gamma^5\gamma^5 = \mathbb{1}_4$ and $M_{\pi^0}^2 = (\boldsymbol{p}+\boldsymbol{q})^2 = 2m_\nu^2 + 2\boldsymbol{p}\cdot\boldsymbol{q}$, we have for $m_\nu^2 << M_{\pi^0}^2$:

$$\begin{aligned} |\mathscr{M}|^2 &= 2G_F^2 F_\pi^2 m_\nu^2\ \text{Tr}(\not{p}\not{q}) = 2G_F^2 F_\pi^2 m_\nu^2\ \text{Tr}(p_\mu \gamma^\mu p_\nu \gamma^\nu) = \\ &= 2G_F^2 F_\pi^2 m_\nu^2\ \text{Tr}(p_\mu p_\nu \frac{1}{2}\{\gamma^\mu, \gamma^\nu\}) = 2G_F^2 F_\pi^2 m_\nu^2\ \text{Tr}(p_\mu p_\nu g^{\mu\nu}) = \\ &= 8G_F^2 F_\pi^2 m_\nu^2 \boldsymbol{p}\cdot\boldsymbol{q} = 4_F^2 F_\pi^2 m_\nu^2 M_{\pi^0}^2. \end{aligned} \tag{1.23}$$

From (1.18), (1.19) and (1.23) we have partial decay width for $\pi^0 \to \nu\bar{\nu}$:

$$\begin{aligned}\Gamma_{\nu\bar{\nu}} &= \frac{1}{8\pi}\frac{M_{\pi^0}}{2}\sqrt{1-\frac{4m_\nu^2}{M_{\pi^0}^2}}\frac{4G_F^2F_\pi^2m_\nu^2M_{\pi^0}^2}{M_{\pi^0}^2} \\ &= \frac{1}{4\pi}\sqrt{1-\frac{4m_\nu^2}{M_{\pi^0}^2}}G_F^2F_\pi^2m_\nu^2M_{\pi^0}.\end{aligned} \tag{1.24}$$

1.4.3 Branching ratio evaluation

Because $BR(\pi^0 \to \gamma\gamma) = (98.823 \pm 0.034)\%$, where

$$BR(\pi^0 \to \gamma\gamma) = \frac{\Gamma_{\gamma\gamma}}{\Gamma_{\text{all}}}, \tag{1.25}$$

we can approximate $\Gamma_{\text{all}} \approx \Gamma_{\gamma\gamma}$ for $\Gamma_{\nu\bar{\nu}}$. Then

$$\frac{\Gamma_{\nu\bar{\nu}}}{\Gamma_{\gamma\gamma}} = \frac{\frac{1}{4\pi}\sqrt{1-\frac{4m_\nu^2}{M_{\pi^0}^2}}G_F^2F_\pi^2m_\nu^2M_{\pi^0}}{\frac{1}{(4\pi)^3}\alpha M_{\pi^0}^3\frac{1}{F_\pi^2}} = \left(\frac{4\pi F_\pi^2G_F}{\alpha}\frac{m_\nu}{M_{\pi^0}}\right)^2\sqrt{1-\frac{4m_\nu^2}{M_{\pi^0}^2}} \tag{1.26}$$

and after substituting all constants the upper limit on the branching ratio is

$$BR(\pi^0 \to \nu\bar{\nu}) = \frac{\Gamma_{\nu\bar{\nu}}}{\Gamma_{\gamma\gamma}} < 5 \cdot 10^{-10} \tag{1.27}$$

for mass of the ν_τ. The amplitude (1.20) is in the case of Majorana neutrinos twice bigger than for Dirac neutrinos because the final state particles are identical. Therefore the branching ratio for the Majorana case would also be twice bigger [4].

2. Layout of NA62 experiment

The NA62 experiment is a particle physics experiment at CERN laboratory which is located on the border between France and Switzerland near Geneva. The European Organization for Nuclear Research known as CERN (Conseil Européen pour la Recherche Nucléaire) operates the largest particle physics laboratory in the world containing several accelerators.

"The accelerator complex at CERN is a succession of machines that accelerate particles to increasingly higher energies. Each machine boosts the energy of a beam of particles, before injecting the beam into the next machine in the sequence. In the Large Hadron Collider (LHC) – the last element in this chain – particle beams are accelerated up to the record energy of 6.5 TeV per particle. Most of the other accelerators in the chain have their own experimental halls where beams are used for experiments at lower energies.

The proton source is a simple bottle of hydrogen gas. An electric field is used to strip hydrogen atoms of their electrons to yield protons. Linac 2 (linear accelerator), the first accelerator in the chain, accelerates the protons to the energy of 50 MeV. The beam is then injected into the Proton Synchrotron Booster (PSB), which accelerates the protons to 1.4 GeV, followed by the Proton Synchrotron (PS), which pushes the beam to 25 GeV. Protons are then sent to the Super Proton Synchrotron (SPS) where they are accelerated to 450 GeV and then injected to the two beam pipes of the LHC." [25]

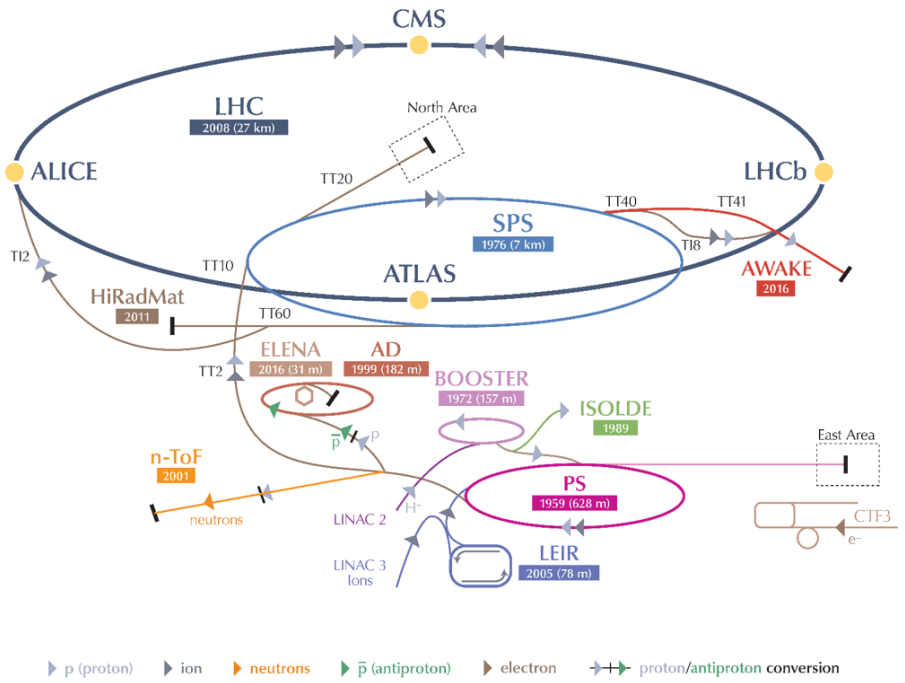

Figure 2.1: CERN's accelerators complex [25].

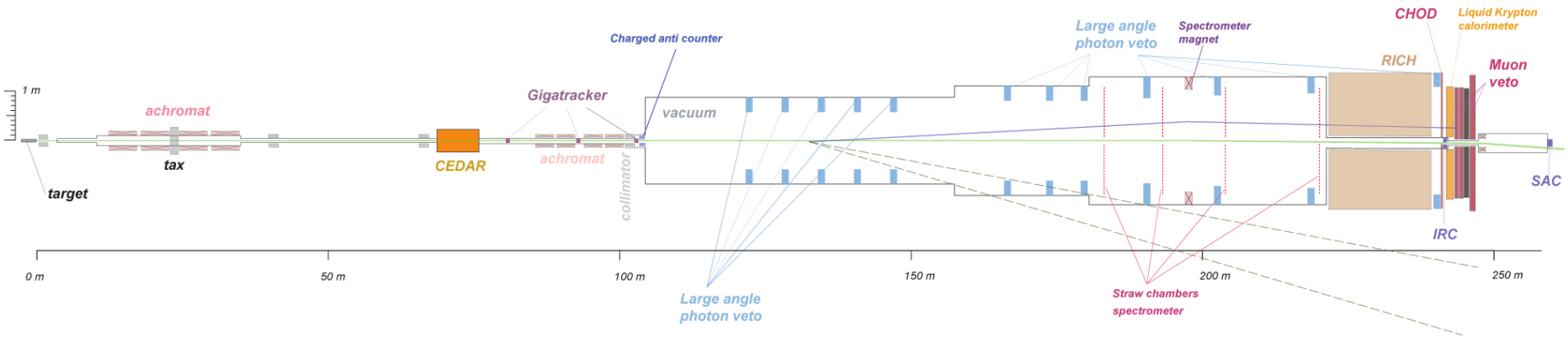

Figure 2.2: NA62 setup [3].

2.1 The aim of NA62

NA62 is one of the fixed-targed experiments located in the Prévessin (France) site, called North Area. The main purpose of the NA62 experiment is to study rare kaon decays. In present configuration the main goal is to measure the ultra-rare decay $K^+ \to \pi^+ + \nu + \bar{\nu}$ and collecting about 80 of these events in two years [3]. Theoretical branching ratio (from Standard Model) for this decay is $BR(SM) = (9.11 \pm 0.72) \cdot 10^{-11}$ [6].

The experiment itself can be subdivided in two parts. The region where undecayed kaons are tagged and beam momentum is measured, called 'upstream region', and 'downstream region' where products of decay are identified and their momenta are measured, see the NA62 layout in the figure 2.2.

2.2 Beam line

The primary proton beam ($1.1 \cdot 10^{12}$ protons/s) at 400 GeV/c taken from SPS accelerator impinges beryllium target T10 and generates secondary high-intensity (750 MHz) hadron beam containing about 6% of K^+. A triplet of radiation-hard quadrupole magnets (Q1, Q2, Q3) collects large angle of particles and is followed by an achromat selecting beam momentum around 75 GeV/c. The archomat consists of four dipole magnets. The first two magnets displace the beam by 110 mm from original axis and keep it parallel. Then the beam passes through a set of apertures TAX1 and TAX2, which select momentum about 75 GeV/c and absorb unwanted particles. Next two magnets of achromat return the beam onto the original axis. A following triplet of quadrupoles (Q4, Q5, Q6) focuses the beam and finally muons of both signs are swept aside using three 2 m long dipole magnets [13].

2.3 KTAG/CEDAR

The KTAG or CEDAR (Cherenkov Differential counter with Achromatic Ring) is a Cherenkov type detector. As K^+ comprise about 6% of the beam and the rest are mostly pions and protons which cannot be efficiently separated from the beam there is a need for a particle identification detector. The KTAG tags kaons very precisely with time resolution below 100 ps and efficiency of kaon identification of 98% [14].

The CEDAR is filled with nitrogen gas at pressure about 1.7 bar. The amount of material in the path of the beam can be decreased by using of hydrogen gas. Thus for the upcoming runs (starting in 2017), KTAG will be filled with hydrogen gas at pressure of 3.6 bar. For given relativistic velocity of the beam, the angle of Cherenkov light is a function of the mass of a particle.

Cherenkov light is reflected by a spherical mirror at the end of the vessel back on the diaphragm at the beginning, so only light of specific particle type has the right angle to reach the slit. There is a sequence of 8 quartz windows, lens

and spherical mirrors to transfer the light to 8 collecting sections of cones which can be seen on the figure 2.3. Coincidence of at least 6 of them indicate passage of kaon.

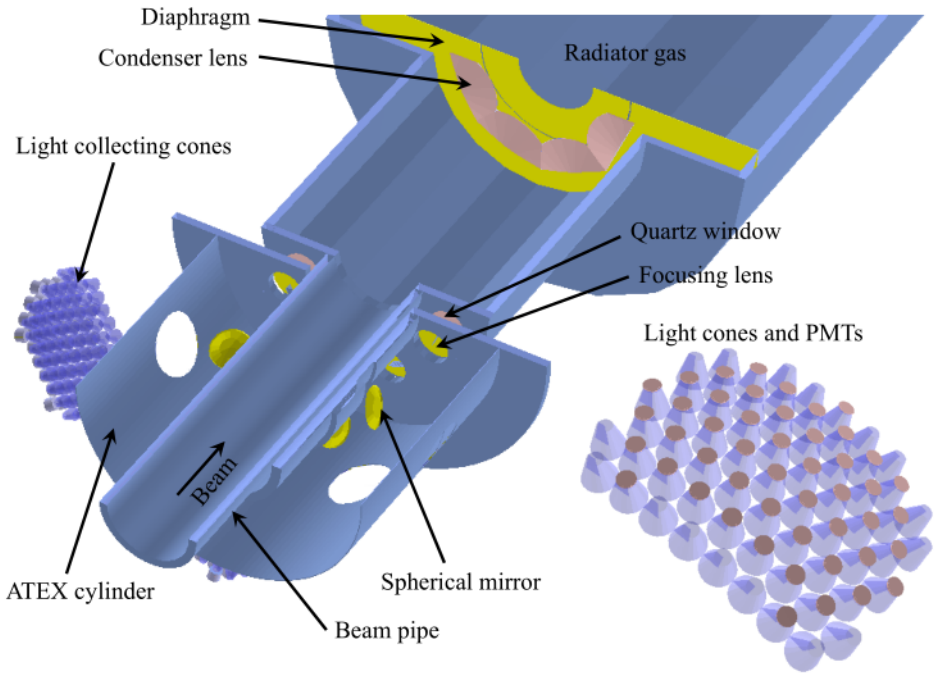

Figure 2.3: KTAG/CEDAR detector [3].

2.4 GTK

The GigaTracker (GTK) is a silicon pixel spectrometer and measures momentum, time and angle of the passing beam. Accuracy is essential here because together with momentum from downstream spectrometer for decayed kaons we can get the missing invariant mass with level at 10^5. Required time resolution is below 200 ps.

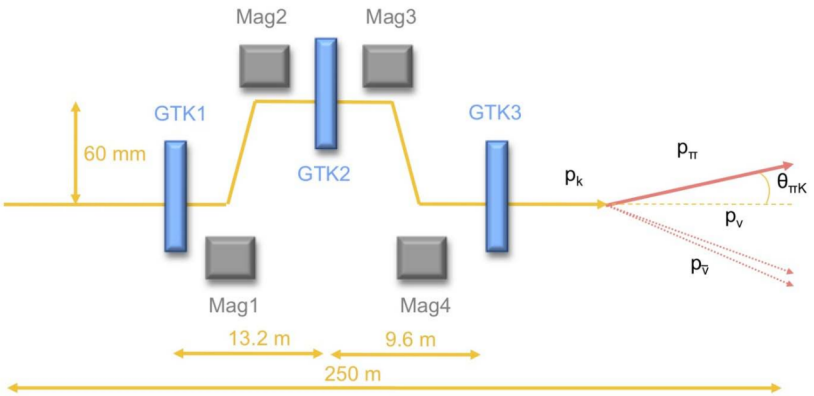

Figure 2.4: GigaTracker setup [15].

The GTK consists of three stations with four dipole magnets among them, see figure 2.4. Each station is made of one silicon pixel detector with 18000 pixels

on area 63.1 × 29.3 mm. The pixel detector consists of ten chips in two rows, each chip is 40 × 45 pixels. The GTK is exposed to high rate of radiation (750 MHz), see figure 2.5. Lifetime of the detector is increased by cooling and higher bias voltage.

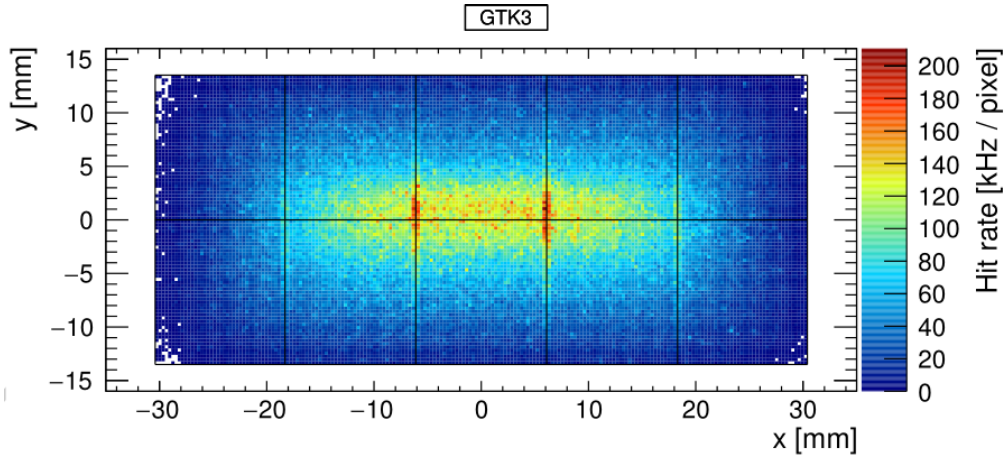

Figure 2.5: GigaTracker station [15].

Magnetic field from dipole magnets deflects charged particles to the second station and back to the axis of the beam line. The layout is set to measure momentum around 75 GeV/c. The real momentum can be derived from the particle displacement in the central station with respect to other two stations [15].

2.5 CHANTI

Particle interactions in the last GTK station are not swept away by the magnetic field like in the first two stations and can produce additional background. For this case there is CHANTI (The Charged Anti-Coincidence Detector) between the GTK3 station and the beginning of the decay region.

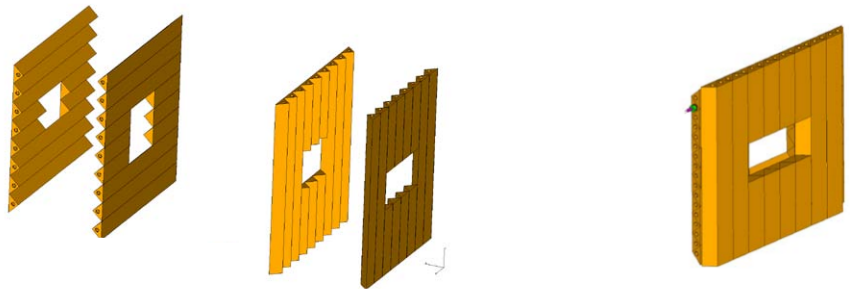

Figure 2.6: CHANTI station construction [16].

The CHANTI consists of six hodoscope stations, each of 300 × 300 mm. A single station is made by 48 bars triangular in cross section. One plane of bars for X and one for Y coordinate, as can be seen in the figure 2.6. Each bar has a polystyrene scintillator with an optical fibre in the middle. Ends of the fibre

are connected to photomultipliers and signal from possible incoming particle is detected.

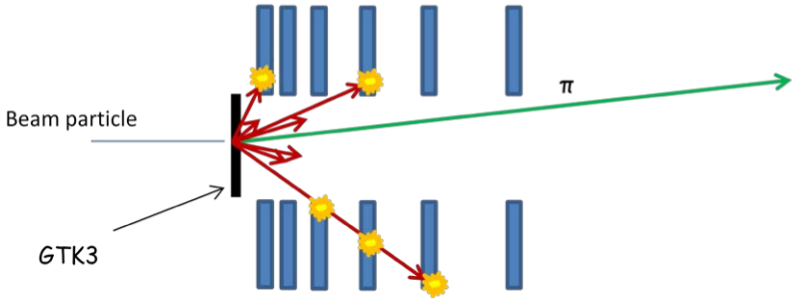

Figure 2.7: CHANTI detector layout [16].

Single CHANTI station locations are chosen to cover the acceptance of the decay region, so any possible inelastic interactions cannot make background, see figure 2.7. The first station is 28 mm from GTK3 station and is covered in the vessel with the GTK station [16].

2.6 Decay region and LAVs

About 18% of tagged kaons with momentum measured by the GTK decay in a 60 m long region also called 'blue tube' due to the cover color. 'Blue tube' is the first part of cca 117 m long evacuated tank with vacuum at pressure about 10^{-6} mbar.

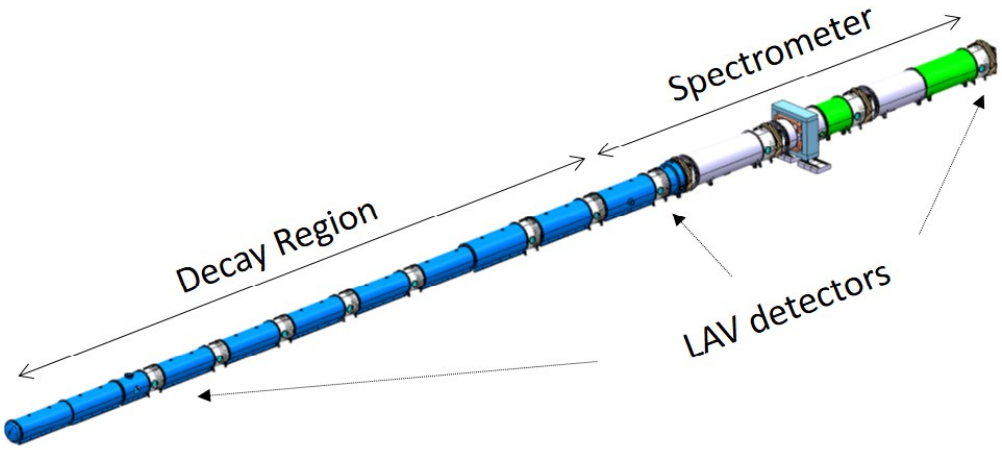

Figure 2.8: Decay region scheme [3].

The beam is in this long region deflected by the so called 'blue field' mostly composed of Earth magnetic field. Final reconstructed results of the track has to be corrected due to the blue field. The blue field correction is $\Delta\theta \sim 35$ μrad for a 25 GeV/c track [17].

The decay region tube is widening with the beam. The diameter at the beginning is 1.92 m and 2.4 m in the end. Because of events where photons are radiated in wide angles ($8 \div 50$ mrad), photon detectors LAV (Large Angle Veto) are placed in the full length of the region, see figure 2.8. There are 12 LAV stations, where last station is operated in the air, just before calorimeter. The LAV station's diameter increases just as increases the diameter of the tube. The setup of one LAV station is in the figure 2.9.

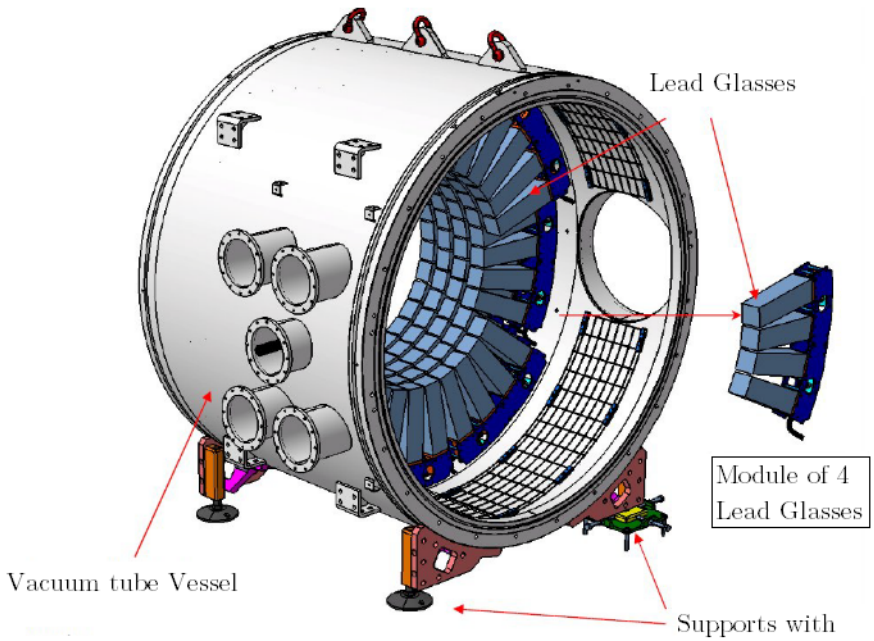

Figure 2.9: Photon veto detector [17].

Each station has lead glass blocks on the edge where possible passing particle leaves signal which is detected. Blocks are located in several mutually shifted rows to cover the whole border of the station.

2.7 Straw Spectrometer

The Straw spectrometer occupies last 35 m of the 117 m long evacuated tank. The first station is placed 25 m from the fiducial region, see figure 2.10.

The spectrometer has four identical stations with a dipole magnet providing vertical magnetic field of 0.38 T between the second and the third station. The first two stations provides vector of the charged track and together with the deflection from the magnetic field the momentum of the track can be measured.

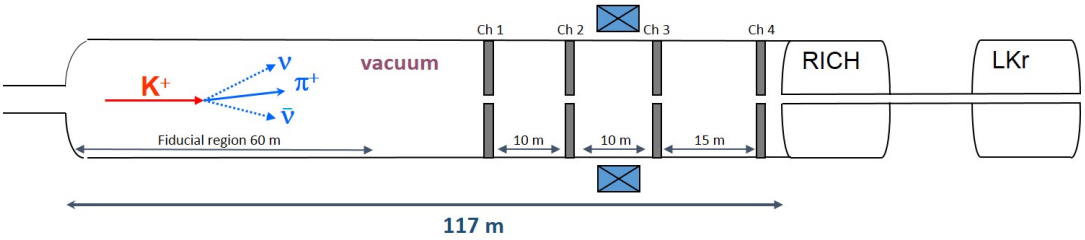

Figure 2.10: Straw spectrometer location [3].

Every station is composed of four planes. Each pair of stations provides vector of charged track. The first two planes (vertical and horizontal) and another two planes rotated by 45° provides more precise measurement of coordinate for one particle and this layout prevents ambiguities if two particles hit the station in the same time, see figure 2.11 [18].

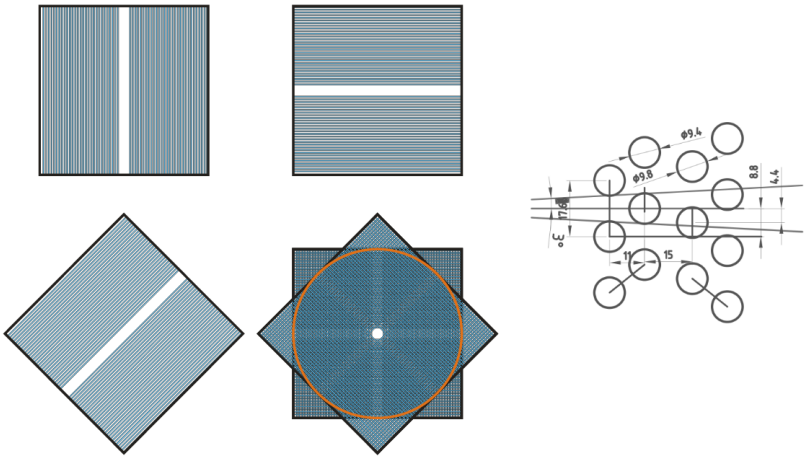

Figure 2.11: Straw spectrometer station [18].

Every plane has 1,792 straws staggered in four rows to cover all possible angles, and leaving place for beam pipe in the middle, as can be seen in the figure 2.11. Straws are placed in the vacuum tank and themselves are filled with 30% of CO_2 and 70% of argon at atmospheric pressure. The straws are made of a very thin (36 μm) PET foil to minimize scattering. Straws are coated from the inside by two metal layers as a cathode, and has an anode wire in the middle with electric field between anode and cathode, so passing particle can be detected through ionization of the filling gas.

2.8 RICH

Ring Imaging Cherenkov Counter (also called 'RICH') is used to separate pions from muons between 15 and 35 GeV/c momentum with time resolution less then 100 ps and also produces the L0 trigger for charged downstream track.

The RICH is a 17.5 m long cylindrical vessel (see figure 2.12) filled with the neon gas at constant pressure of 990 mbar. The vessel has four sections which diameter increases backwards against the direction of the beam. The entrance and exit windows have conical shape and are made of two and four mm thick aluminium, where entrance window separates the vessel from the vacuum of the decay region [19].

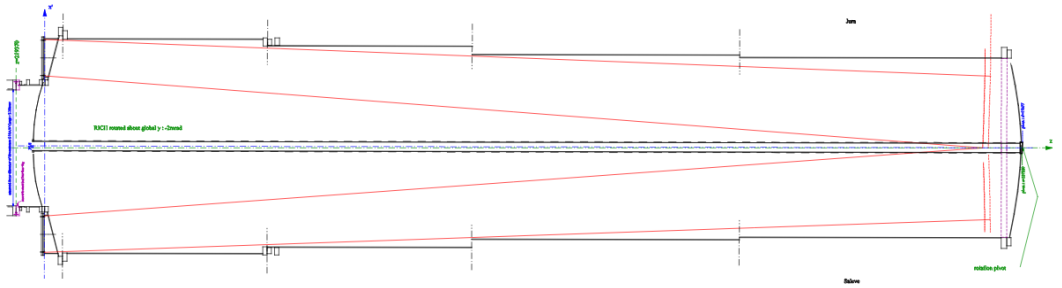

Figure 2.12: RICH layout [19].

To increase the resolution and to keep photomultipliers out of the active area the downstream end of the vessel of 3.2 m diameter is filled with mosaic of 20 spherical mirrors which reflect the cone of Cherenkov light backwards onto the photomultipliers, see figure 2.13. Half of the mirrors points left and half right of the beam pipe. The inner side of the vessel is covered with black epoxy painting to avoid reflection of the Cherenkov light from it [19]. In 2014 - 2015 runs for 86% pion efficiency a 1.3% muon survival probability was observed [3].

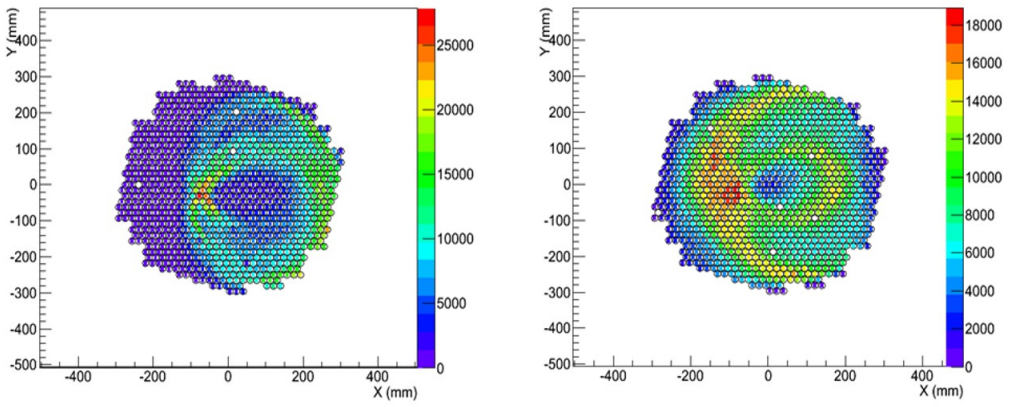

Figure 2.13: Photomultipliers on the left and right side illuminated by Cherenkov light [3].

2.9 CHOD/NewCHOD

Charged particle hodoscopes (CHOD) are fast scitillator detectors which provides impact point position of passing particle. Due to the fast readout they are also used for L0 trigger. There are two CHOD detectors, the New CHOD detector immediately behind the RICH, followed by the last LAV station and the original NA48-CHOD further downstream.

The NA48-CHOD has two planes of 64 scintillator slabs with photomultipliers on the ends with space left around the beam pipe. The track crossing rate at the CHOD is around 13 MHz, see figure 2.14 [20].

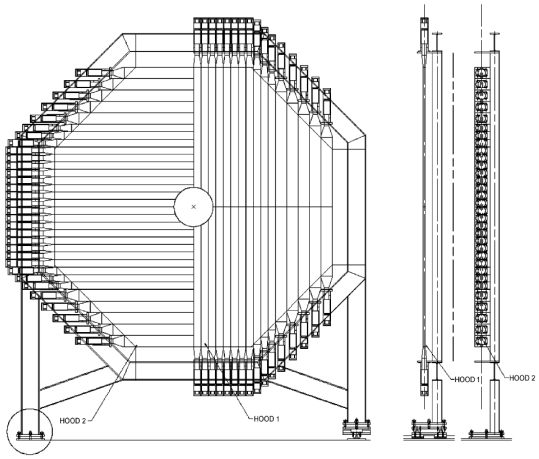

Figure 2.14: CHOD scheme [3].

The NewCHOD is a single plane of scintillator tiles mostly 135 mm or 200 mm wide with bigger density of tiles around beam pipe, as can be seen in the figure 2.15 [3].

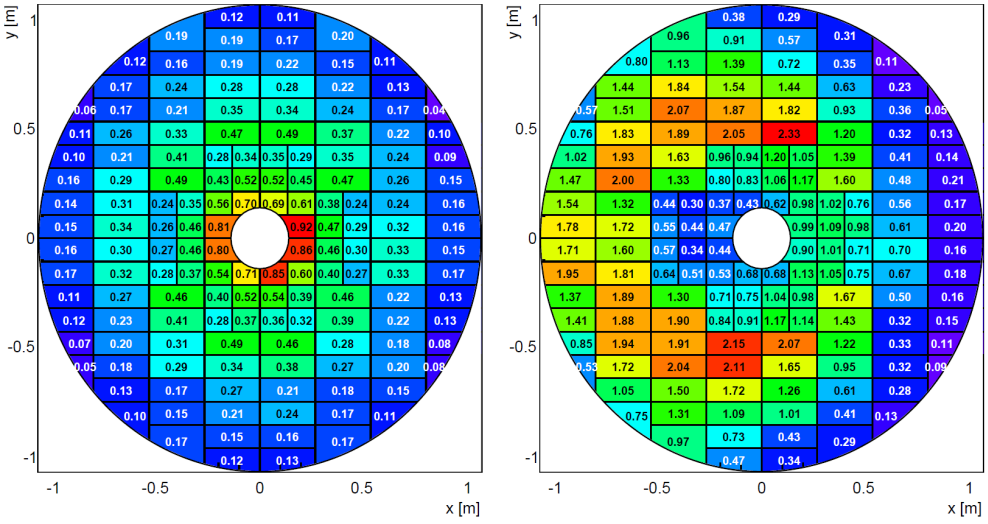

Figure 2.15: NewCHOD scheme [3].

2.10 LKr

The LKr is an electromagnetic calorimeter filled with 9 m^3 of liquid krypton at 130 K which is placed inside the cryostat. The active area of LKr is composed of a single plane with 13248 cells about 2×2 cm with Cu-Be electrodes. The radius of the LKr is 128 cm and first 8 cm are left for beam pipe [3].

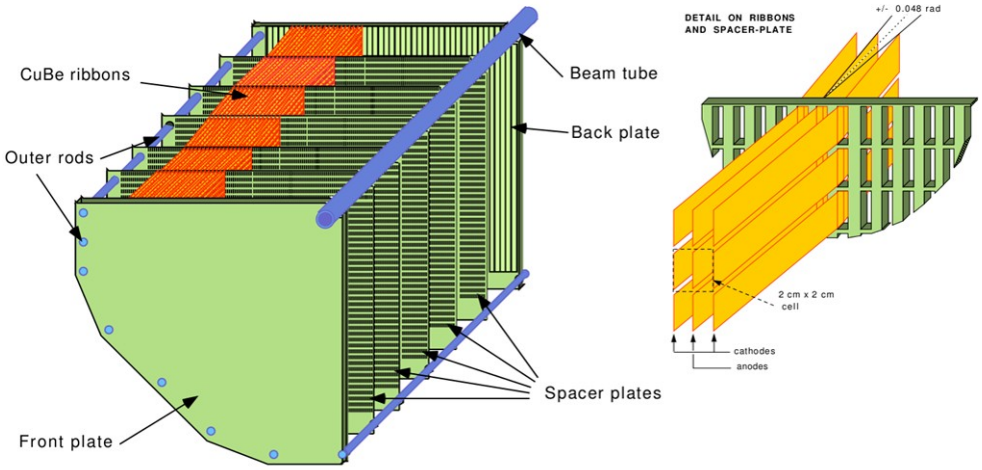

Figure 2.16: Left: One LKr quadrant layout, Right: LKr cells detail [3].

Alternating electrodes filling the plane are oriented with the beam axis but slightly deflected. They change the direction of the deflection several times to avoid inefficiency for very flat tracks close to the anodes - 'zig-zag' longitudinal shape of cells, see figure 2.16.

2.11 MUV

The MUV is a system of three independent detectors serving as a muon veto (MUV3) and two hadronic calorimeters (MUV1 and MUV2) - can be seen the figure 2.17. MUV3 also provides fast muon veto trigger L0 [21].

The MUV1 is an iron-scintillator sandwich calorimeter of twelve vertical and twelve horizontal layers covering a plane of 260×260 cm. Each scintillator strip is 260×6 (or 4) $\times 1$ cm. The scintillators are connected to photomultipliers through wave-length shifting (WLS) fibers [3].

The MUV2 is refurbished original NA48 hadron calorimeter. It is very similar to MUV1. It has 22 layers of strips instead of 24 and readout photomultipliers are connected directly to scintillators.

The iron wall of 80 cm is placed between the MUV2 calorimeter and the MUV3 to stop remaining particles in the acceptance of previous detectors. The wall is thick enough to leave just muons, which are detected in the MUV3 veto detector directly downstream. It is composed of 22×22 cm tiles with two photomultipliers

placed 21 cm behind each tile. They cover the angle for scintillation photons and also detect Cherenkov radiation if muon passes through the photomultiplier windows for more precise timing [3].

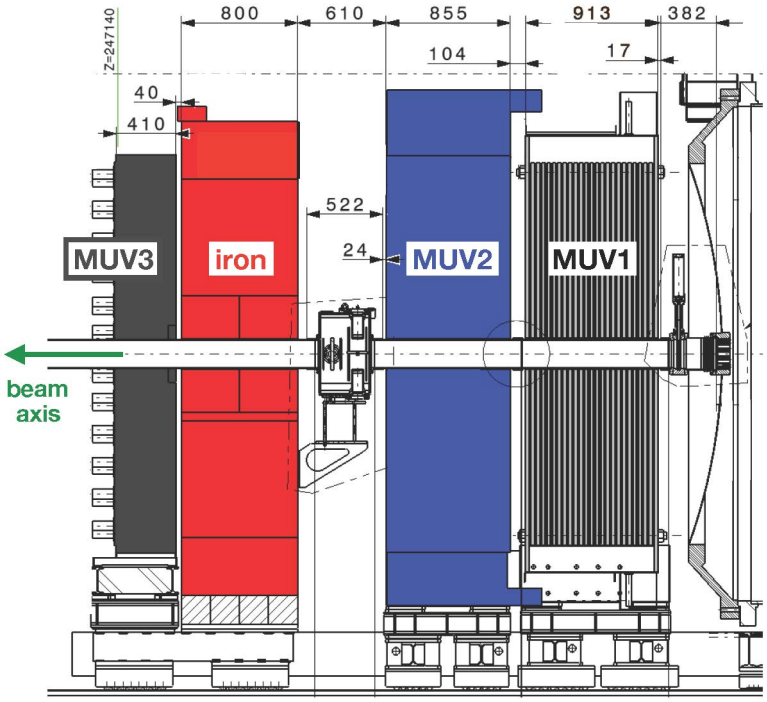

Figure 2.17: MUV detectors layout [3].

2.12 Additional Veto Detectors

Small angle veto detectors (SAV) the Small angle calorimeter (SAC) and the Intermediate ring calorimeter (IRC) detect photons radiated at low angles out of the range of the LKr.

The IRC is placed between CHOD and LKr and covers radius from 7 cm to 14 cm. It is composed of layers of lead and scintillators.

The magnet placed behind MUV3 on the beam line region deviates charged beam particles to the dump which is situated off the axis. Neutral particles like photons remain in the axis and are detected in the SAC which construction is similar to IRC's. It is the shashlik detector type and has 70 alternating layers of scintillator and lead [17].

3. Trigger system

The high beam rate of (750 MHz) with an estimated 10 MHz rate of decays in detector dictates a need for a high-performance trigger system to maximize the high quality data collection. A unified trigger and data acquisition (TDAQ) system has been used in NA62. The TDAQ system is composed of a single hardware trigger level (L0) and high level triggers (L1 and L2) together reducing the data rate to 10 kHz which meets the bandwidth of the data flow for permanent storage tapes.

3.1 L0 trigger

The L0 trigger is designed to reduce the data flow to the maximum rate of 1 MHz and latency below 1 ms which by default comprises only a small set of sub-detectors but can be easily extended to most of them. This set of detectors consists of: **CHOD**, **NewCHOD**, **RICH**, **LAV**, **MUV3** and calorimeters (**LKr**, **MUV1** and **MUV2**). Channels of the first five detectors are connected to the Time-to-Digital-Converter (TDC) chips on TEL62 boards, see figure 3.1.

Figure 3.1: A TEL62 board equipped with two TDC boards and the quad gigabit board [3].

Due to a large data rate of calorimeters, their channels are connected to the calorimeter readout (CREAM) system at first, which saves data into local temporary buffers.

CHOD L0 trigger provides selection of just single-track events with impact time correction, which is required due to the length of NA48 CHOD scintillator bars. It is used in L0 as an independent stream (control trigger)

NewCHOD L0 trigger is used for the appraisal of multi-track events

RICH L0 trigger is based on hit multiplicity for any charged track above signal threshold.

LAV L0 trigger is meant to veto events with photons or muons within the LAV system acceptance which requires using of all LAV stations, each with individual TEL62 board and final inter-communication among these boards.

MUV3 L0 trigger provides fast muon veto which is important condition for $K^+ \to \pi^+\nu\bar{\nu}$ decay. All 296 MUV3 channels are connected to a single TEL62 board equipped with three TDC boards.

The calorimeter L0 trigger (**CAL-L0**) is used to select events with a π^+ in the final state and to veto events with π^0 which is one of the most dominant events. The readout is provided through the CREAM system and the CAL-L0 prepares time-ordered lists of reconstructed clusters which are sorted by the L0 Trigger Processor.

3.2 High level triggers

While the maximum rate of L0 trigger is 1 MHz a considerable data reduction has to be made to meet the 10 kHz requirements of the permanent data storage. NA62 uses two high level software triggers L1 and L2.

3.2.1 L1 trigger

The L1 trigger reduces the data rate to 100 kHz and uses **KTAG**, **CHOD** and **LAV** detectors separately from L0 trigger.

KTAG trigger selects only the kaon events and additionally demands signal in four from eight KTAG sectors in the referential time of the L0 trigger.

CHOD trigger uses cut for a maximum of six active slabs in time and rejects multitrack events. It also can be used to reject $K^+ \to \pi^+\pi^0$ event with photon conversion.

LAV trigger is applied on events which passed the L0 trigger and rejects those events with activity in more then three LAV stations. It is used to reduce the background of $K^+ \to \pi^+\pi^0$ events with photons emitted at large angles.

3.2.2 L2 trigger

The L2 trigger reduces the data rate by another factor 10 to the final 10 kHz rate suitable for the permanent data storage. It is a software trigger based on partial track reconstruction. It combines information from Straw spectrometer and the GTK to find a vertex of the event, which position is used for another data cut [3].

4. Data analysis

The data from individual runs of experiment are reconstructed and saved on EOS, which is disk-based, low-latency storage system (over 120 PB of raw disk space) at CERN. The reconstruction itself works on level of single detectors and consists in matching of signals from individual channels, specifically hits in individual subdetectors, e.g. photomultipliers.

Generally this matching is based on time and space closeness of individual hits where these reconstruction algorithms are being progressively upgraded. As a result of reconstruction, data are divided on events which are subdivided into trees for individual detectors. In these trees are *candidates* (matched hits) for passed particles and their parameters (e.g. mean time, location) in subfolders. The next level of analysis is matching of candidates between individual detectors for every event.

Since we are looking for very rare events with undetectable particles, we have to reconstruct all possible detectable background events, which will be then eliminated from the whole set of events.

4.1 Reconstruction strategy

As we are looking for $\pi^0 \to \nu\bar{\nu}$ event, the subject of this part of thesis is reconstruction of dominant $\pi^0 \to \gamma\gamma$ event from $K^+ \to \pi^+\pi^0$ decay. The reconstruction is based on matching of detectable K^+ track (upstream track) with π^+ (downstream) track and then looking for γ tracks from kinematics as $\pi^0 \to \gamma\gamma$ decay happens de facto immediately.

The following analysis was performed on data from NA62 experiment, run 6610 in 2016 with reconstruction version r1421.

4.1.1 Tracks reconstruction

The upstream track reconstruction simply consists in matching of CEDAR kaon tagged candidates with GTK candidates based on time difference in both detectors. As the time resolution for KTAG is $\sigma_T(KTAG) \approx 80$ ps and for GTK is $\sigma_T(GTK) \approx 100$ ps, $200 - 300$ ps difference time condition for matching is achievable. The trajectory of the beam can be reconstructed from momentum and position from GTK.

The downstream track reconstruction is essential for the description of kinematics. The trajectory is known from momentum and positions in the Straw spectrometer and can be refined through matching with candidates in CHOD and NewCHOD. The result of matching can be seen in the histogram in the figure 4.1, where the raw cut (the circle) is given as a distance of the CHOD candidate from the track and the main cut (the square) is on the discriminant given as a linear combination of differential positions and differential times between

the downstream track and the CHOD candidate. The downstream track referential time is then also represented by the CHOD with the $\sigma_T(CHOD) \approx 250$ ps resolution.

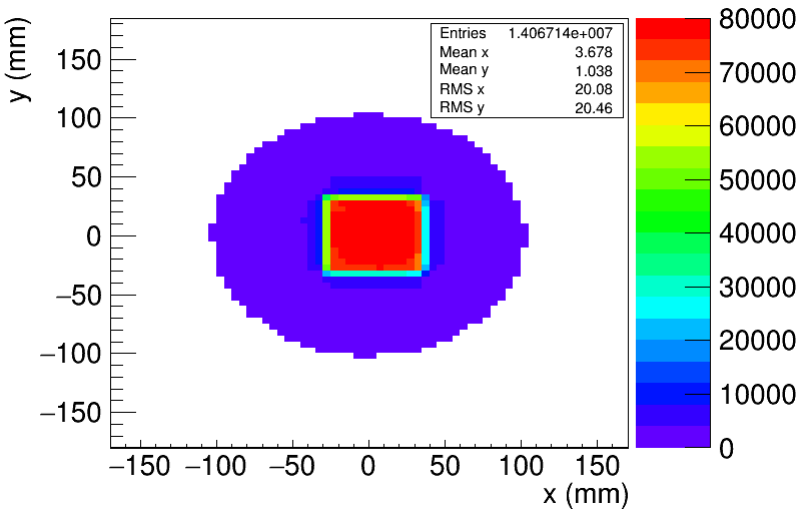

Figure 4.1: Distance between the position of CHOD candidate and track projection.

The π^+ track distinguishing from other charged tracks (like muon) is initially performed by the RICH, where the radius of radiated circle is given by the β factor, thus for given momenta, radii for differently massive particles can be distinguished. See characteristics in figure 4.2, where are muon and pion curves, the kaon background separately and a flat curve of light electrons. The RICH time resolution is $\sigma_T(RICH) \approx 150$ ps and using the time of the RICH candidates are those matched with the downstream track.

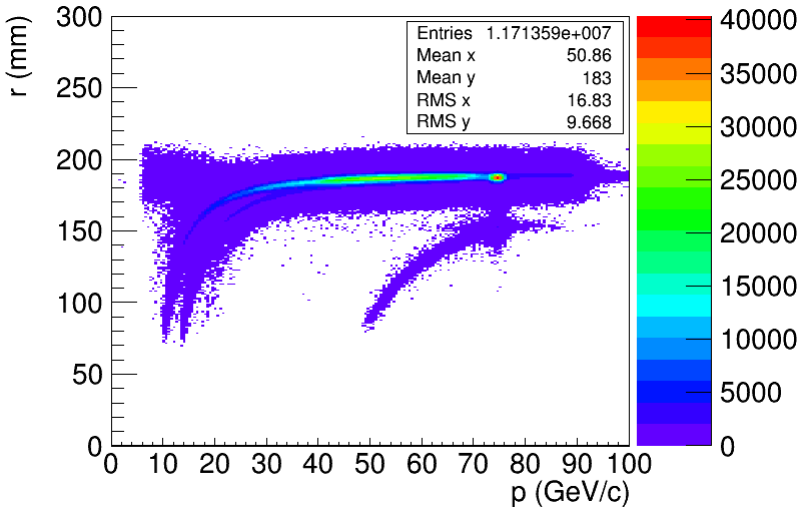

Figure 4.2: Radius of ring in RICH for given momentum.

4.1.2 Event reconstruction

If individual tracks belong to the same event, they must have a common vertex. Variable named CDA (closest distance of approach) is used to find common vertex and to assess quality of the match between tracks. It is defined as a shortest distance between two skew lines. The upstream track belonging to the downstream track (or downstream tracks in case of multitrack event) is chosen as the candidate with the smallest CDA. With the current precision of the setup and detectors $CDA \approx 1.5$ mm is reachable, see histogram in the figure 4.3 with a raw cut on $CDA < 9$ mm. Another condition is that the decay must take place in the decay area, which makes claim on the z coordinate of vertex $(105 < z < 180)$ m (due to the setup of the experiment).

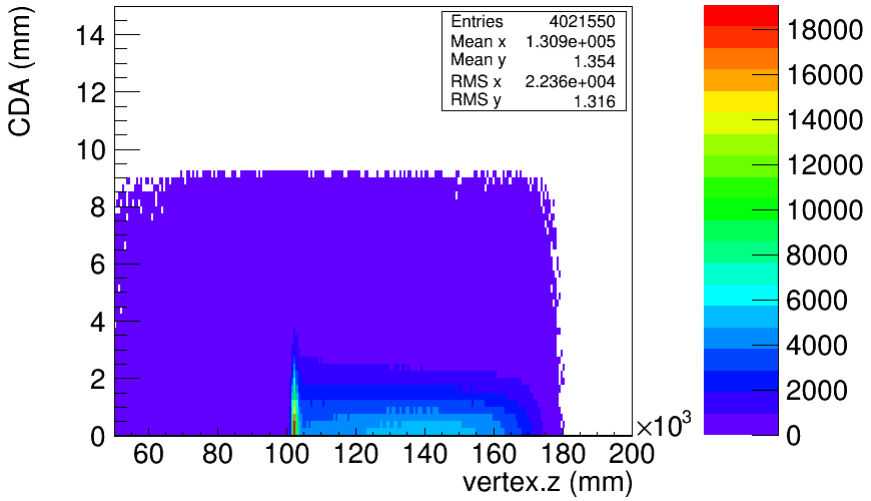

Figure 4.3: z vertex coordinate and CDA of tracks.

4.2 $\pi^0 \to \gamma\gamma$ decay reconstruction

To reconstruct uncharged tracks of γ, we have to select the $K^+ \to \pi^+\pi^0$ decay. Thus we have to select a singletrack decay and from known four-momenta of kaon and pion reconstruct the missing invariant mass as $m^2_{miss} = P^2_K - P^2_\pi$ (π^+ and K^+ masses and momenta are known [6]), see histogram in figure 4.4.

For our decay, we are looking for squared mass of π^0 which is given as $m^2_{\pi^0} = 0.01822$ GeV$^2/c^4$ [6], we can see a peak in figure 4.4. However we can also see a peak for mouns (on the left), three-pion decays (on the right) and an indistinguishable background of K_{e3} and $K_{\mu 3}$ decays. Following cuts on upstream and downstream tracks were applied to clear this sample:

- cut on CDA: $CDA < 3$ mm;
- cut on vertex position: as we can see in figure 4.3, there are lots of events with collisions at GTK3 station, thus we use cut for z vertex coordinate $z > 115$ m together with eliminating events with signal in the CHANTI detector

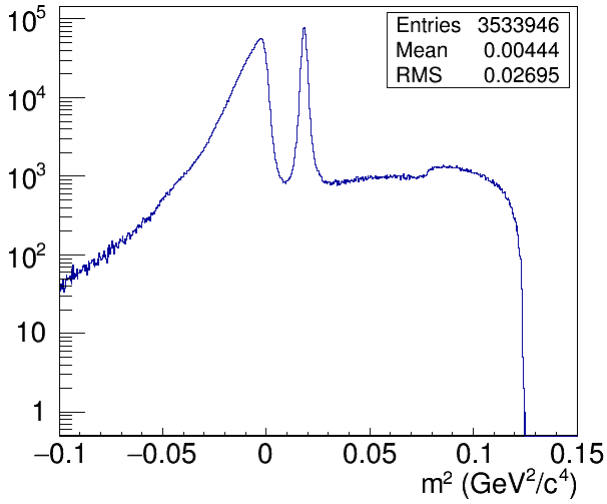

Figure 4.4: Missing invariant mass.

- to eliminate events with particles emitted in angles out of acceptance of calorimeters, we use cut on events with signal in photon veto detectors (LAV, IRC and SAC);
- to minimize events with muons, we also use a cut on events with signal in MUV3.

As we can see on histogram in the figure 4.5, our cuts were effective and we have mostly events with $K^+ \to \pi^+\pi^0$ decay with two orders lower background noise. Most of the remaining background is eliminated with cut for invariant mass of π^0. The four-momentum of π^0 is then simply given as $P_{\pi^0} = P_{K^+} - P_{\pi^+}$.

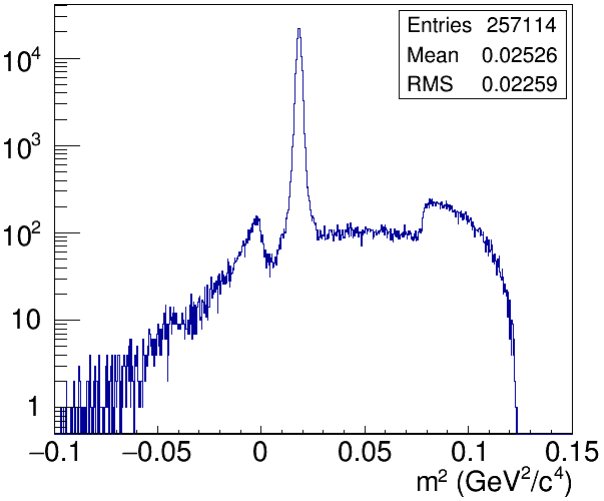

Figure 4.5: Missing invariant mass after quality cuts.

For the reconstruction of uncharged γ tracks we will employ the LKr. At first we want to select the pion cluster at LKr, which is simply done by projection of the pion vector on the calorimeter and matching with the closest cluster, in

the same way have done for the CHOD. Following conditions on this cluster are set:

- the distance of cluster from pion projection is below 40 mm;
- possible dead cells of the cluster are in minimum distance of 20 mm from the seed of the cluster as we want the main part of the cluster fully reconstructed;
- other clusters in LKr are at least 200 mm distant;
- the energy of the pion cluster is at least 1 GeV to eliminate the muon background, see the histogram in the figure 4.6.

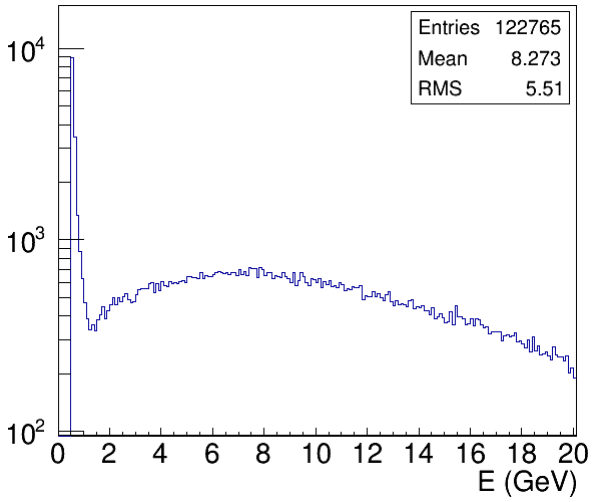

Figure 4.6: Energy of clusters matched with pions.

To increase the quality of the event, another conditions are set:

- all LKr clusters are active in maximum time difference of 5 ns;
- the energy of every photon cluster is above 2 GeV to reduce the background and to overcome the possibility of wrong cluster reconstruction;
- π^+ momentum is between 5 and 60 GeV/c to reduce the probability of emitting very low energetic photons in the $\pi^0 \to \gamma\gamma$ decay.

The outcome of this part of thesis is the efficiency of LKr for the dominant $\pi^0 \to \gamma\gamma$ event which is fundamental for further analysis of the $\pi^0 \to \nu\bar{\nu}$ decay. As we want the decay with three particles in the final state, we take events with maximally three active clusters where one belongs to the π^+ and randomly chosen second cluster should belong to the photon γ_1. The same conditions on the dead cell distance and the distance of the cluster from other clusters as on the pion cluster are set.

As a photon is massless and we know its energy and position of vertex, we have its four-momentum P_{γ_1}. The four-momentum of the second photon is then

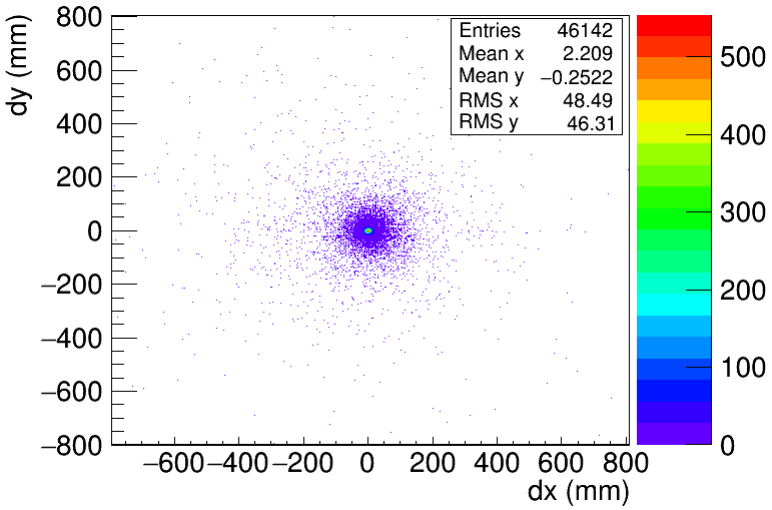

Figure 4.7: Distance of second γ cluster from expected position.

simply $P_{\gamma_2} = P_{\pi^0} - P_{\gamma_1}$ and we can also check that we have a photon track from its zero invariant mass.

To match the second photon with the second cluster a presence of the second cluster in 300 mm distance from the expected position is needed, due to the electromagnetic shower overlaping, see the distribution in the figure 4.7. Also the difference between expected and found energy of the second cluster can be seen in figure 4.8. In case of just one photon cluster, the alternative reconstruction algorithm (auxiliary) for LKr candidates is used to find extra clusters.

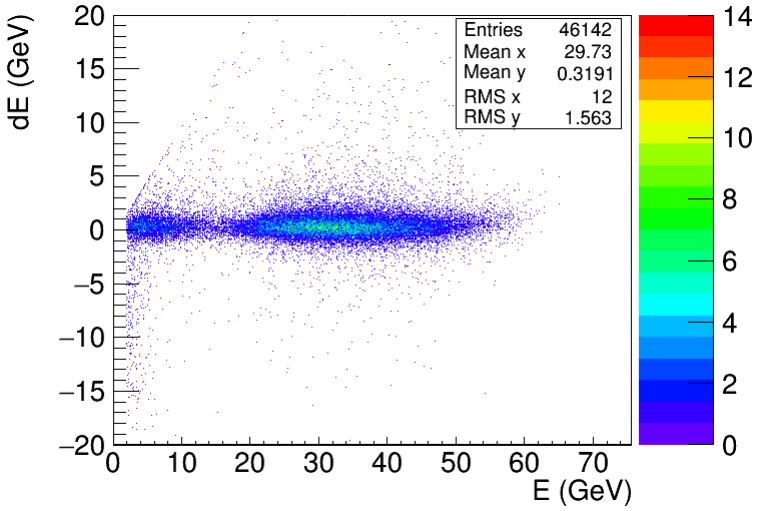

Figure 4.8: Difference between expected and real energy of second cluster as a function of energy of the first photon.

The efficiency of LKr is given as a ratio of matched γ clusters and all γ clusters, see figure 4.9 for the distribution of energies of individual clusters and figure 4.10 for the efficiency of LKr.

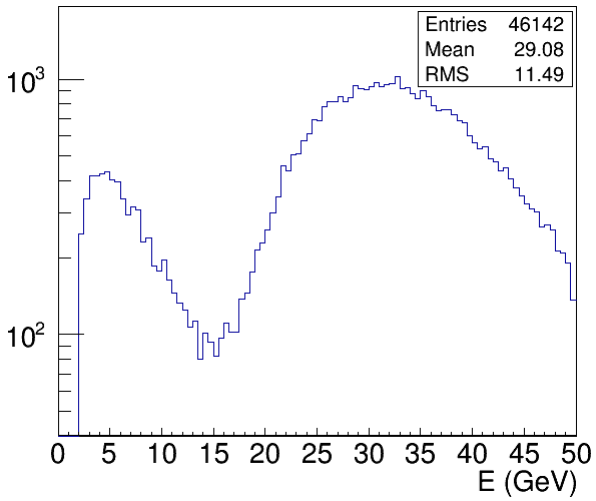

Figure 4.9: Energy of all γ clusters

As we can see the efficiency for higher energies is satisfying. We have there only one unmatched event among the order of 10^4 events, which gives us 10^{-4} inefficiency. For better understanding of inefficiency, the analysis should be performed further on a bigger amount of data. Nevertheless the result for lower energies is very bad and we have a huge event loss for lower energies.

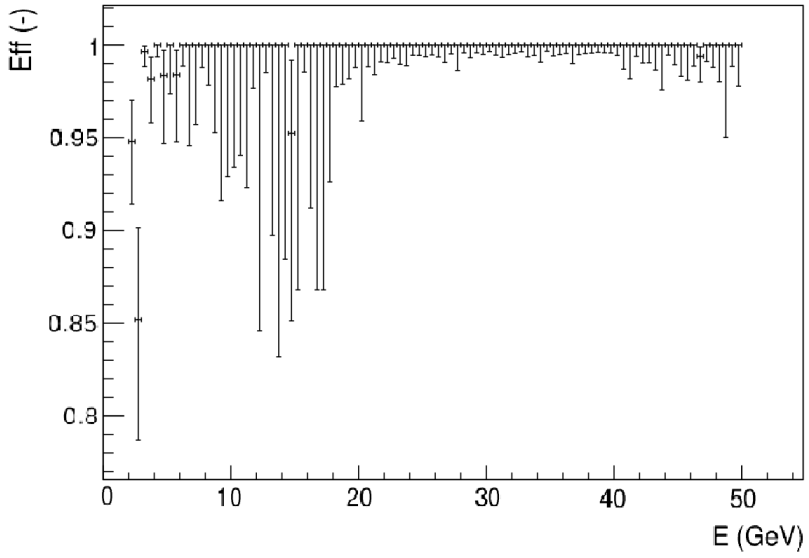

Figure 4.10: LKr efficiency.

Conclusion

In the first part of the thesis the upper limit on the branching ratio of our studied decay $\pi^0 \to \nu\bar{\nu}$ has been evaluated using established description of the decay kinematics. Using LO correction for chiral anomaly we have obtained a result:

$$BR(\pi^0 \to \nu\bar{\nu}) = \frac{\Gamma_{\nu\bar{\nu}}}{\Gamma_{\gamma\gamma}} < 5 \cdot 10^{-10}.$$

In the second part the setup of the apparatus used to measure this decay has been described. We have also created an analyser for data collected on NA62 experiment to obtain reconstruction of the dominant decay of the π^0 meson ($\pi^0 \to \gamma\gamma$) and evaluated the efficiency of the calorimeter (LKr) for this decay.

The output of the analysis for higher energy photons was satisfying (inefficiency of LKr in order of 10^{-4}), nevertheless the analyser was inefficient for lower energies and huge data loss in this region was observed. This issue can be solved by improving the analyser to be more sensitive to lower energies because the region is still far behind the achievable performance of the LKr. Then the analysis could be used for further study of the rare $\pi^0 \to \nu\bar{\nu}$ decay.

Bibliography

[1] A. J. Buras, D. Buttazzo, J. Girrbach-Noe & R. Knegjens. [$K^+ \to \pi^+\nu\bar{\nu}$ *and* $K_L \to \pi^0\nu\bar{\nu}$ *in the Standard Model: Status and Perspectives*]. **JHEP 1511**, (2015). Available from:
arXiv:1503.02693[hep-ph]

[2] A. V. Artamonov, *et al.* (BNL - E949 Collaboration). [*Study of the decay* $K^+ \to \pi^+\nu\bar{\nu}$ *in the momentum region* $140 \leq P(\pi) \leq 199\text{MeV}/c$]. Phys. Rev. D **79**, 092004, (2009). Available from:
arXiv:0903.0030[physics.ed-ph]

[3] B. Bloch-Devaux, *et al.* NA62 Collaboration. [*The Beam and detector of the NA62 experiment at CERN*]. (2017). Available from:
arXiv:1703.08501[physics.ins-det]

[4] A. V. Artamonov, *et al.* (BNL - E949 Collaboration). [*Upper Limit on the Branching Ratio for the Decay* $\pi^0 \to \nu\bar{\nu}$]. Phys. Rev. D **72**, 091102, (2005). Available from:
arXiv:hep-ex/0506028

[5] G. Elert, The Physics Hypertextbook, *The Standard Model*. [online]. 1998-2017. [Accessed 8 May 2017]. Available from:
http://physics.info/standard/

[6] C. Patrignani, *et al.* (Particle Data Group). [*Review of particle Physics*]. Chin. Phys. C **40**, 100001, (2016)

[7] K. Kumerički (University of Croatia, Zagreb, Croatia). [*Feynman Diagrams for Beginners*]. (2016). Available from:
arXiv:1602.04182[physics.ed-ph]

[8] S. Scherer (Institut f. Kernphysik, Mainz, Germany). [*Introduction to Chiral Perturbation Theory*]. Adv. Nucl. Phys. **27**, (2003) 277. Available from:
arXiv:hep-ph/0210398

[9] K. Kampf. [*On decays of light unflavoured pseudoscalar mesons*]. LU TP 11-35, (2011). Available from:
arXiv:1109.4370[hep-ph]

[10] J. L. Rosner, *et al.*. [*Leptonic Decays of Charged Pseudoscalar Mesons*]. EFI 15-21, FERMILAB-PUB-15-384-T, (2015). Available from:
arXiv:1509.02220[hep-ph]

[11] K. Kampf & B. Moussallam. [*Chiral expansions of the* π^0 *lifetime*]. Phys. Rev. D **79**, 076005, (2009). Available from:
arXiv:0901.4688[hep-ph]

[12] CERN, *The accelerator complex*. [online]. 2012. [Accessed 25 April 2017]. Available from:
http://cds.cern.ch/record/1997193

[13] NA62 Collaboration, *Beam line - Technical design*. 2010. [Accessed 25 April 2017]

[14] NA62 Collaboration, *KTAG - Technical design*. 2010. [Accessed 25 April 2017]

[15] NA62 Collaboration, *GTK - Technical design*. 2010. [Accessed 25 April 2017]

[16] NA62 Collaboration, *CHANTI - Technical design*. 2010. [Accessed 25 April 2017]

[17] NA62 Collaboration, *The Photon Veto Detectors - Technical design*. 2010. [Accessed 25 April 2017]

[18] NA62 Collaboration, *StrawTracker - Technical design*. 2010. [Accessed 25 April 2017]

[19] NA62 Collaboration, *RICH - Technical design*. 2010. [Accessed 25 April 2017]

[20] NA62 Collaboration, *CHOD - Technical design*. 2010. [Accessed 25 April 2017]

[21] NA62 Collaboration, *MUV - Technical design*. 2010. [Accessed 25 April 2017]

[22] Wikipedia, *The Standard Model*. [online]. 2017. [Accessed 25 April 2017]. Available from: `https://en.wikipedia.org/wiki/Standard_Model`

[23] Scientific explorer, *All About the Particles in Physics*. [online]. 2011. [Accessed 25 April 2017]. Available from: `http://sciexplorer.blogspot.cz/2011/12/all-about-particles-in-physics.html`

[24] J. S. Denker, *Quarks → Mesons → Nonet*. [online]. 2015. [Accessed 25 April 2017]. Available from: `https://www.av8n.com/physics/quark-meson-nonet.htm`

[25] CERN, *Cern's Accelerator Complex*. [online]. 2016. [Accessed 25 April 2017]. Available from: `https://espace.cern.ch/acc-tec-sector/default.aspx`

List of Abbreviations

CKM - Cabibbo-Kobayashi-Maskawa mixing matrix
SM - Standard Model of particle physics
QED - Quantum Electrodynamics
QCD - Quantum Chromodynamics
EWT - Electroweak Theory
BR - Branching Ratio
χPT - Chiral Perturbation Theory
LO - Leading Order
CERN - Conseil Européen pour la Recherche Nucléaire
LHC - Large Hadron Collider
Linac - Linear accelerator
PSB - Proton Synchrotron Booster
PS - Proton Synchrotron
SPS - Super Proton Synchrotron
CEDAR - Cherenkov Differential counter with Achromatic Ring
GTK - GigaTracker
CHANTI - Charged Anti-Coincidence Detector
LAV - Large Angle Veto
RICH - Ring Imaging Cherenkov Counter
CHOD - Charged particle Hodoscope
LKr - Liquid Krypton Calorimeter
MUV - Muon Veto
WLS - Wave-Length Shifting fibres
SAV - Small Angle Veto
SAC - Small Angle Calorimeter
IRC - Intermediate Ring Calorimeter
TDAQ - Trigger and Data Acquisition system
TDC - Time-to-Digital Converter
CREAM - Calorimeter Readout System
CAL-L0 - Calorimeter L0 trigger
CDA - Closest Distance of Approach

A personal goal of the author was that the total number of pages of this thesis is exactly 42 to answer the Ultimate Question of Life, the Universe, and Everything